Three-Dimensional Static Modeling of the Lumbar Spine

Ernur Karadogan, Ph.D. and **Robert L. Williams II**, Ph.D.
Mechanical Engineering Department, Ohio University, Athens OH

Keywords: human lumbar spine, three-dimensional static modeling, Robotic Lumbar Spine, RLS

Abstract

This paper presents three-dimensional static modeling of the human lumbar spine to be used in the formation of anatomically-correct movement patterns for a fully cable-actuated robotic lumbar spine (RLS) which can mimic in vivo human lumbar spine movements to provide better hands-on training for medical students. The mathematical model incorporates five lumbar vertebrae between the first lumbar vertebra and the sacrum, with dimensions of an average adult human spine. The vertebrae are connected to each other by elastic elements, torsional springs and a spherical joint located at the inferoposterior corner in the mid-sagittal plane of the vertebral body. Elastic elements represent the ligaments that surround the facet joints and the torsional springs represent the collective effect of intervertebral disc which plays a major role in balancing torsional load during upper body motion and the remaining ligaments that support the spinal column. The elastic elements and torsional springs are considered to be nonlinear. The nonlinear stiffness constants for six motion types were solved using a multi-objective optimization technique. The quantitative comparison between the angles of rotations predicted by the proposed model and in the experimental data confirmed that the model yields angles of rotation close to the experimental data. The main contribution is that the new model can be used for all motions while the experimental data was only obtained at discrete measurement points.

1 Introduction

The art of palpation is usually taught by using human patients who are palpated by the instructor for demonstrative purposes. Medical students watch the process and palpate each other, generally with limited dysfunctions. It is difficult to find and demonstrate patients for every dysfunction taught. There exists no assessment device to objectively evaluate clinical palpation of students. To enhance palpation teaching assessment, a cable-actuated robotic lumbar spine (RLS) is currently under development [1]. The current study involves lumbar spine movement patterns to define RLS motions under different loading conditions.

Studies for mathematical modeling of the thoracic, lumbar and thoracolumbar spine include [2-12]. [8] developed the first static 3D model for spine nonlinear force analysis. The authors used a stiffness method considering the vertebrae as rigid bodies connected with deformable elements having axial, torsional, bending and shear resistance. In a continuation [9], the authors emphasized the kinematic constraints role of facet joints. Facets and the ligaments carry loads in bending and torsion. [10] performed a lumbar spine static simulation based on experimental data in [11]. They simulated ligamentous and non-ligamentous soft tissue using linear springs, whereas nonlinear behavior is expected. [12] used a L3-L4 segment finite element model to analyze the facet orientation sensitivity and the initial joint gap between facets. Both parameters affected the facet load.

In this paper, a model of the human lumbar spine using nonlinear elastic elements and torsional springs based on experimental data is proposed. The purpose is to create a model that accurately estimates the movement patterns of the lumbar

vertebrae under externally-applied forces and moments. The experimental data used presents vertebral motion at discrete values. The proposed model estimates movement patterns continuously, i.e. for any applied moment. The model's validation and simulation results are presented.

2 Methods

2.1 Construction of the Lumbar Spine Geometry

The lumbar spine geometry has average human dimensions based on experimental data [1]. All geometry parameters have been previously used in the literature, except for the facet plane and facet plane angle. Assuming sagittal symmetry, we define a facet plane that connects the four facet centers. This plane allows the attachment of posterior elements with various dimensions, making the system modular. The facet plane angle is the angle between the facet plane and the vertebral body posterior wall. A cylindrical shape is assumed for vertebral bodies. Figure 1 shows the facet plane angle and cylindrical vertebral body. The lumbar spine geometry is shown in Figure 2.

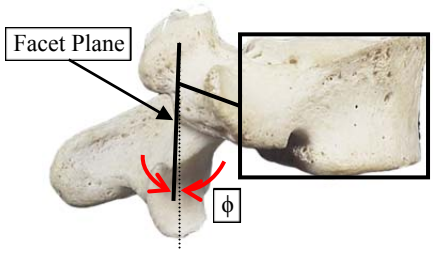

Figure 1. Facet Plane and Angle

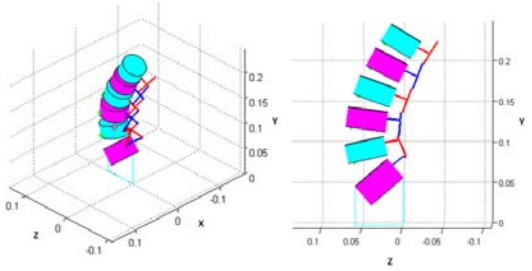

Figure 2. 3D Geometry of the Lumbar Spine [1]

2.2 Mathematical Model

The mathematical model includes five lumbar vertebrae and the sacrum, 10 elastic elements that connect inferior facets of one vertebra to the superior facets of the lower one and 15 torsional springs that represent the collective torque-resisting effects of the intervertebral disc and the ligaments. The significant motion of the vertebrae during spinal movement is rotational [11-13]. Therefore, a spherical joint connects vertebrae. This joint location is critical to provide anatomically-correct motion for each vertebra during overall lumbar movement. The spherical joints are located at the inferoposterior corners of the vertebral bodies because the experimental data used is [13]. In that reference, the inferoposterior corner of each vertebra is the coordinate frame origin for which the rotation angles were recorded.

The equations of static equilibrium for forces and moments are derived for each vertebra using the free-body diagram (Figure 3). Force equilibrium in the base frame {B} can be written as:

$$\sum {}^{B}\mathbf{F}_{i} = m_i\,{}^{B}\mathbf{g} + {}^{B}\mathbf{F}_{srf_i} + {}^{B}\mathbf{F}_{slf_i} + {}^{B}\mathbf{F}_{irf_i} + {}^{B}\mathbf{F}_{ilf_i} + {}^{B}\mathbf{R}_{i} - {}^{B}\mathbf{R}_{i+1} = -\,{}^{B}\mathbf{F}_{ext_i} \tag{1}$$

m_i is the *i*-th vertebra mass, ${}^{B}g = \{0\ -9.81\ 0\}^{T}$ is the gravity vector, ${}^{B}\mathbf{F}_{srf_i}$, ${}^{B}\mathbf{F}_{slf_i}$, ${}^{B}\mathbf{F}_{irf_i}$, ${}^{B}\mathbf{F}_{ilf_i}$ are the forces due to the elastic element connected to the superior right facet, superior left facet, inferior right facet and inferior left facet, and ${}^{B}R_i$ is the spherical joint reaction force. ${}^{B}F_{ext_i}$ is the external force applied to the *i*-th vertebra center of gravity.

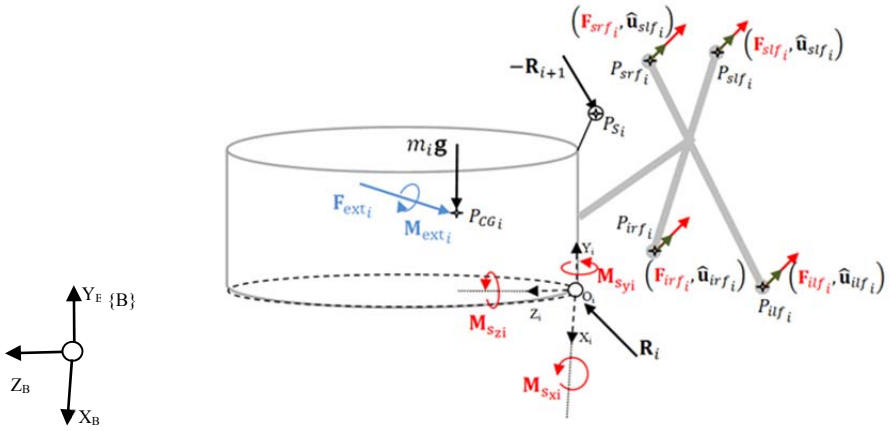

Figure 3. Free-Body Diagram of a Vertebra

As in [13], the external forces are all zero except for one at the uppermost vertebra L1. This 100-Newton compressive force represents partial torso weight. This external force's line of action passes through the centers of gravity of first lumbar and first sacral vertebra during motion. The elastic elements forces connecting the facets in (1) are:

$$\begin{aligned}
{}^{B}\mathbf{F}_{srf_i} &= {}^{B}_{i}R\left(k_{srf_i}\left(\left\|{}^{i}_{i+1}R\,{}^{i+1}\mathbf{P}_{irf_{i+1}} - {}^{i}\mathbf{P}_{srf_i}\right\| - G\right)\right)\,{}^{i}\hat{\mathbf{u}}_{srf_i}\\
{}^{B}\mathbf{F}_{slf_i} &= {}^{B}_{i}R\left(k_{slf_i}\left(\left\|{}^{i}_{i+1}R\,{}^{i+1}\mathbf{P}_{ilf_{i+1}} - {}^{i}\mathbf{P}_{slf_i}\right\| - G\right)\right)\,{}^{i}\hat{\mathbf{u}}_{slf_i}\\
{}^{B}\mathbf{F}_{irf_i} &= {}^{B}_{i}R\left(k_{irf_i}\left(\left\|{}^{i}_{i-1}R\,{}^{i-1}\mathbf{P}_{srf_{i-1}} - {}^{i}\mathbf{P}_{irf_i}\right\| - G\right)\right)\,{}^{i}\hat{\mathbf{u}}_{irf_i}\\
{}^{B}\mathbf{F}_{ilf_i} &= {}^{B}_{i}R\left(k_{ilf_i}\left(\left\|{}^{i}_{i-1}R\,{}^{i-1}\mathbf{P}_{slf_{i-1}} - {}^{i}\mathbf{P}_{ilf_i}\right\| - G\right)\right)\,{}^{i}\hat{\mathbf{u}}_{ilf_i}
\end{aligned} \tag{2}$$

${}^{B}_{i}R$ is the rotation matrix giving the orientation of frame {i} with respect to {B}, using X-Y-Z (α, β, γ) Euler angles:

$$ {}^{\mathrm{B}}_{\mathrm{i}}\mathrm{R} = \begin{bmatrix} \mathrm{c}\beta\mathrm{c}\gamma & -\mathrm{c}\beta\mathrm{s}\gamma & \mathrm{s}\beta \\ \mathrm{s}\alpha\mathrm{s}\beta\mathrm{c}\gamma + \mathrm{c}\alpha\mathrm{s}\gamma & -\mathrm{s}\alpha\mathrm{s}\beta\mathrm{s}\gamma + \mathrm{c}\alpha\mathrm{c}\gamma & -\mathrm{s}\alpha\mathrm{c}\beta \\ -\mathrm{c}\alpha\mathrm{s}\beta\mathrm{c}\gamma + \mathrm{s}\alpha\mathrm{s}\gamma & \mathrm{c}\alpha\mathrm{s}\beta\mathrm{s}\gamma + \mathrm{s}\alpha\mathrm{c}\gamma & \mathrm{c}\alpha\mathrm{c}\beta \end{bmatrix} \tag{3} $$

where $\mathrm{c}\alpha = \cos\alpha$, $\mathrm{c}\beta = \cos\beta$, $\mathrm{c}\gamma = \cos\gamma$, $\mathrm{s}\alpha = \sin\alpha$, $\mathrm{s}\beta = \sin\beta$, $\mathrm{s}\gamma = \sin\gamma$.

The remaining variables in (2) are: G=2 mm [14,15] is the facets joint gap (equal to the unstretched springs length when the lumbar spine is upright), ${}^{\mathrm{i}}\mathbf{P}_{irf_{\mathrm{i}}}$, ${}^{\mathrm{i}}\mathbf{P}_{ilf_{\mathrm{i}}}$, ${}^{\mathrm{i}}\mathbf{P}_{srf_{\mathrm{i}}}$, ${}^{\mathrm{i}}\mathbf{P}_{slf_{\mathrm{i}}}$ are the facet centers position vectors with respect to local vertebral frame {i} (Figure 3), $\mathrm{k}_{\mathrm{srf}}$ is the stiffness constant, and ${}^{\mathrm{i}}\hat{\mathbf{u}}_{srf_i}$ is the unit vector in the local vertebral frame {i} that defines the force line of action in the corresponding elastic element. The remaining forces and stiffness constants are defined similarly.

The static equilibrium equations for the moments about the local frame {i} are:

$$ \begin{aligned} \sum {}^{\mathrm{i}}\mathbf{M}_{\mathrm{i}} \;=\; & {}^{\mathbf{i}}\mathbf{M}_{\mathrm{s}} + \left({}^{\mathrm{i}}\mathbf{P}_{\mathrm{CG_i}} \times {}^{\mathrm{i}}_{\mathrm{B}}\mathrm{R}\, {}^{\mathrm{B}}\mathbf{F}_{\mathrm{ext_i}} \right) + \left({}^{\mathrm{i}}\mathbf{P}_{\mathrm{CG_i}} \times {}^{\mathrm{i}}_{\mathrm{B}}\mathrm{R}\, m_i\, {}^{\mathbf{B}}\mathbf{g} \right) + \left({}^{\mathrm{i}}\mathbf{P}_{srf_{\mathrm{i}}} \times {}^{\mathrm{i}}_{\mathrm{B}}\mathrm{R}\, {}^{\mathbf{B}}\mathbf{F}_{srf_i} \right) \\ & + \left({}^{\mathrm{i}}\mathbf{P}_{slf_{\mathrm{i}}} \times {}^{\mathrm{i}}_{\mathrm{B}}\mathrm{R}\, {}^{\mathbf{B}}\mathbf{F}_{slf_i} \right) + \left({}^{\mathrm{i}}\mathbf{P}_{irf_{\mathrm{i}}} \times {}^{\mathrm{i}}_{\mathrm{B}}\mathrm{R}\, {}^{\mathbf{B}}\mathbf{F}_{irf_i} \right) + \left({}^{\mathrm{i}}\mathbf{P}_{ilf_{\mathrm{i}}} \times {}^{\mathrm{i}}_{\mathrm{B}}\mathrm{R}\, {}^{\mathbf{B}}\mathbf{F}_{ilf_i} \right) \\ & - \left({}^{\mathrm{i}}\mathbf{P}_{\mathrm{S_i}} \times {}^{\mathrm{i}}_{\mathrm{B}}\mathrm{R}\, {}^{\mathrm{B}}\mathbf{R}_{\mathrm{i+1}} \right) \\ = & - {}^{\mathrm{i}}\mathbf{M}_{\mathrm{ext_i}} \end{aligned} \tag{4} $$

${}^{\mathrm{i}}\mathrm{M}_{\mathrm{s}} = \{ {}^{\mathrm{i}}\mathrm{M}_{\mathrm{s_{xi}}} \;\; {}^{\mathrm{i}}\mathrm{M}_{\mathrm{s_{yi}}} \;\; {}^{\mathrm{i}}\mathrm{M}_{\mathrm{s_{zi}}} \}^{\mathrm{T}}$ is the moment vector due to torsional springs attached to the *i*-th vertebra, ${}^{\mathrm{i}}\mathrm{M}_{\mathrm{s_{xi}}} = -\mathrm{k}_{\mathrm{s_{xi}}}\mathrm{q}_{\mathrm{xi}}$ is the moment due to the torsional spring about the x-axis, $\mathrm{k}_{\mathrm{s_{xi}}}$ is the spring constant of the torsional spring about the x-axis and q_{xi} is the angular displacement. ${}^{\mathrm{i}}\mathrm{M}_{\mathrm{s_{yi}}}$ and ${}^{\mathrm{i}}\mathrm{M}_{\mathrm{s_{zi}}}$ are the same way as ${}^{\mathrm{i}}\mathrm{M}_{\mathrm{s_{xi}}}$ using y and z axes. ${}^{\mathrm{i}}\mathrm{P}_{\mathrm{CG}}$ and ${}^{\mathrm{i}}\mathrm{P}_{\mathrm{S}}$ are the position vectors from the local origin to the center of gravity and center of the socket in {i} (Figure 3).

2.3 Experimental Data

The simulation results to validate the proposed model are based on experimental data in [13]. These researchers used fresh-frozen lumbosacral-spine specimens with only ligamentous soft tissue to test lumbar spine mechanical behavior by constructing load-displacement curves for each vertebra under specific loading conditions. Motion was induced by applying pure moments to the first lumbar vertebra. This moment, applied about one of the three axes of rotation, caused spine to flex/extend, bend or rotate axially. The applied moment magnitude was 2.5, 5.0, 7.5 and 10 Nm. The data contained the translation and rotation of each vertebra under the tested loading condition. It is emphasized once more, however, that the rotational motion remained dominant over the translational motion. A load-displacement data example for L3-L4 segment model validation is in Table 1.

Table 1. Experimental Load-Displacement Data for L3-L4 [13]

	External Moment, M_{ext} (Nm)			Motion (°)		
	X	**Y**	**Z**	**X**	**Y**	**Z**
Flexion	2.50	0.00	0.00	5.00	0.00	0.00
	5.00	0.00	0.00	6.00	0.00	0.00
	7.50	0.00	0.00	6.50	0.00	0.00
	10.00	0.00	0.00	7.00	0.00	0.00
Extension	-2.50	0.00	0.00	-1.50	0.00	0.00
	-5.00	0.00	0.00	-2.25	0.00	0.00
	-7.50	0.00	0.00	-2.00	0.00	0.00
	-10.00	0.00	0.00	-2.75	0.00	0.00
Left Torque	0.00	2.50	0.00	0.75	0.50	0.25
	0.00	5.00	0.00	1.13	1.00	0.38
	0.00	7.50	0.00	1.25	1.63	0.50
	0.00	10.00	0.00	1.75	1.75	0.63
Right Torque	0.00	-2.50	0.00	0.50	-0.88	-0.38
	0.00	-5.00	0.00	-0.25	-1.75	-0.50
	0.00	-7.50	0.00	0.50	-1.88	-0.75
	0.00	-10.00	0.00	0.63	-2.00	-1.00
Right Bending	0.00	0.00	2.50	0.75	0.75	3.10
	0.00	0.00	5.00	1.50	0.80	4.00
	0.00	0.00	7.50	1.75	0.80	4.75
	0.00	0.00	10.00	1.50	1.25	5.00
Left Bending	0.00	0.00	-2.50	-0.25	-0.60	-3.50
	0.00	0.00	-5.00	0.60	-1.00	-4.50
	0.00	0.00	-7.50	1.50	-1.00	-5.00
	0.00	0.00	-10.00	1.40	-1.25	-5.50

3 Results

In the first stage of validation, the nonlinear stiffness constants for the elastic elements and the torsional springs are calculated for static equilibrium using the experimental data for six motion types (flexion/extension, right/left torque, right/left bending). The static equilibrium equations (1) and (4) for all vertebrae (30 equations total) are solved simultaneously numerically. The static equilibrium problem is converted into a multi-objective optimization problem by minimizing the equilibrium equations for each vertebra. The rotation angles for each vertebra for all six motion types and four different external moment values (2.5, 5.0, 7.5 and 10.0 Nm) are known [13]. The stiffness constants are calculated for each externally applied moment. Due to space limitations, solved stiffness constants only for flexion are presented in Table 2. The results for the remaining motion types can be found in [14].

Table 2. Nonlinear Stiffness Constants for Flexion

Vertebra	External Moment (Nm)†	k_{s_x} (Nm/rad)	k_{s_y} (Nm/rad)	k_{s_z} (Nm/rad)	k_{srf} (N/m)	k_{slf} (N/m)	k_{irf} (N/m)	k_{ilf} (N/m)
L5	2.50	36.40	0.00	0.00	390.26	386.46	0.77	0.75
	5.00	27.88	0.00	0.00	376.52	373.70	1.44	1.32
	7.50	26.53	0.00	0.00	271.03	274.90	1.17	48.26
	10.00	24.08	0.00	0.00	350.54	350.54	1.48	1.48
L4	2.50	0.00	0.00	0.00	418.41	418.47	390.26	386.46
	5.00	0.01	0.00	0.00	353.15	347.99	376.52	373.70
	7.50	0.00	0.00	0.00	241.43	238.49	271.03	274.90
	10.00	0.03	0.00	0.00	257.88	257.88	350.54	350.54
L3	2.50	0.00	0.00	0.00	178.34	172.89	418.41	418.47
	5.00	0.13	0.00	0.00	113.76	111.09	353.15	347.99
	7.50	0.00	0.00	0.00	65.50	40.42	241.43	238.49
	10.00	0.00	0.00	0.00	48.21	48.21	257.88	257.88
L2	2.50	0.01	0.00	0.00	10.63	10.74	178.34	172.89
	5.00	0.06	0.00	0.00	0.07	0.00	113.76	111.09
	7.50	0.00	0.00	0.00	1.10	1.11	65.50	40.42
	10.00	0.04	0.00	0.00	1.08	1.08	48.21	48.21
L1	2.50	75.26	0.00	0.00	0.00	0.00	10.63	10.74
	5.00	102.03	0.00	0.00	0.00	0.00	0.07	0.00
	7.50	122.56	0.00	0.00	0.00	0.00	1.10	1.11
	10.00	139.47	0.00	0.00	0.00	0.00	1.08	1.08

† X component of the external moment. Y and Z components are all zero for flexion motion.

After obtaining the stiffness constants at available loading conditions, curve fitting is applied to calculate stiffness values for any moment (not limited to the discrete experimental data). This curve fitting is based on a third degree polynomial:

$$k = a * M_{ext}^3 + b * M_{ext}^2 + c * M_{ext} + d \tag{5}$$

k is the stiffness constant (k_{s_x}, k_{s_y}, k_{s_z} for torsional springs or k_{srf}, k_{slf}, k_{irf}, k_{ilf} for elastic elements), M_{ext} is the nonzero component of the moment vector applied to the uppermost vertebra L1, and a, b, c and d are the polynomial coefficients.

The second stage of validation is the comparison of the model and experimental data. The model is tested under moments 2.50, 3.35, 4.20, 5.00, 5.85, 6.70, 7.50, 8.35, 9.20 and 10.00 Nm using the stiffness constants obtained in the first stage by using (5). The validation moment values include the experimental data moments. Figure 4 shows the model output for the L3-L4 segment. The model closely follows the angle values for common moment values tested, i.e. 2.5, 5.0, 7.5 and 10 Nm, typical of all our results.

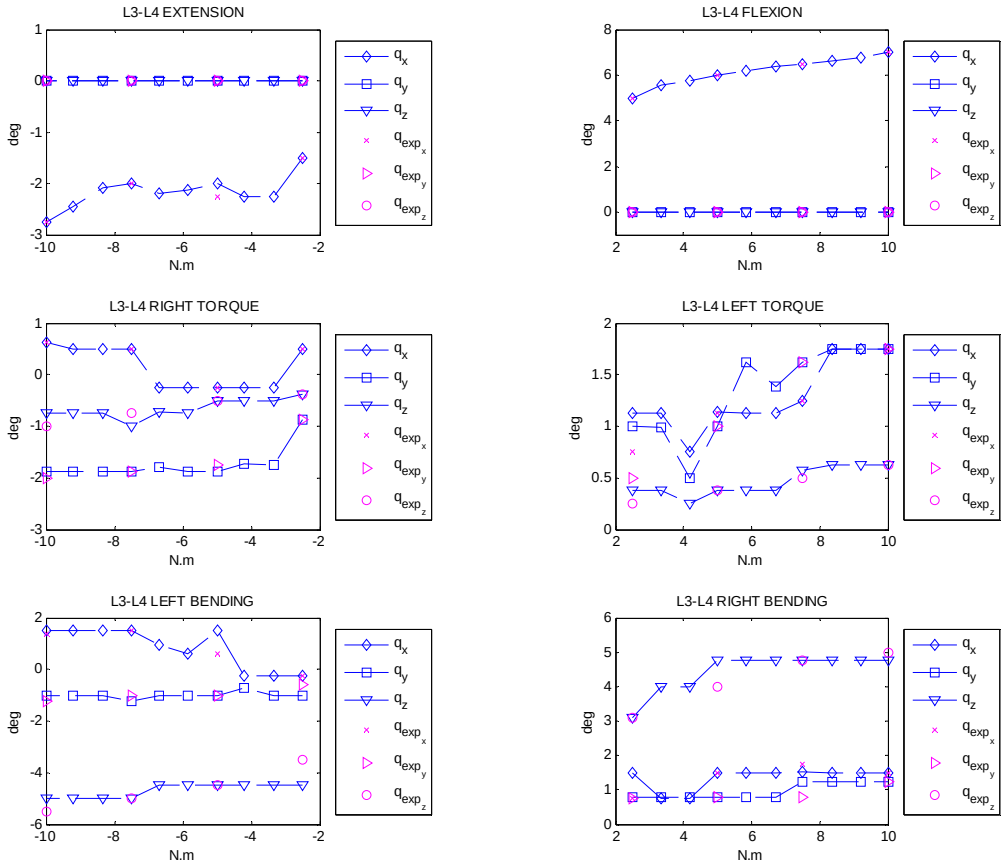

Figure 4. Model vs. Experimental Data (L3-L4 shown)

Figure 5 shows the absolute errors between the angles of rotation predicted by the model and experimental data for the L3-L4 segment.

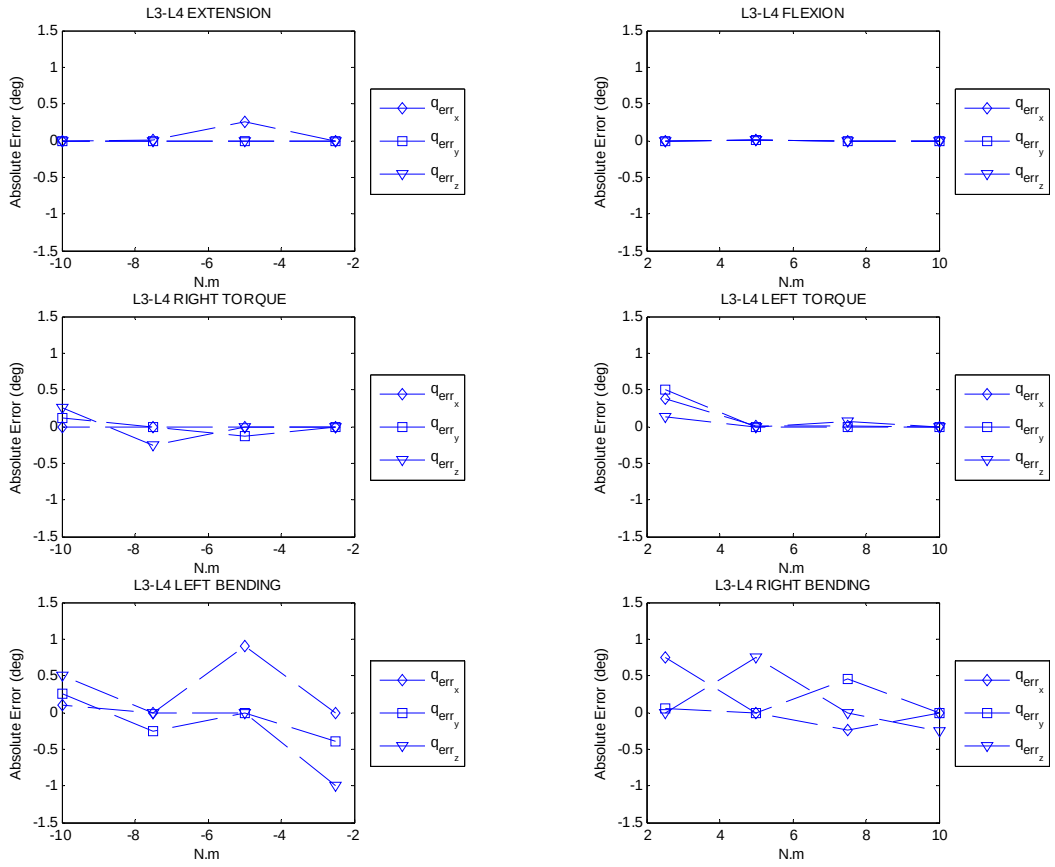

Figure 5. Absolute Error in Model Estimation of the Experimental Data (L3-L4 shown)

4 Discussion

A mathematical model that is validated by comparing its results to experimental data becomes a powerful tool since the change of parameters would be sufficient to modify a specific configuration or a loading condition without repeating the experiment. The purpose of this study was to create a tool to predict normal anatomically-correct movement patterns for the human lumbar spine. The proposed model, as seen from the results, closely follows the experimental data when they are available and predicts the movement patterns for six different motion types continuously for applied moment within 0-10 Nm.

The experimental or model data relating to the motion of the spine varies from specimen to specimen [15]. For instance, when the same motion model is tested with ligament stiffness values chosen from different experimental studies, the intersegmental rotation (L3-L4) results are significantly affected [16]. This variability makes it even harder to compare results. In this model, the effect of the ligaments of the spine except for the facet capsulary ligaments was incorporated into three parameters (stiffness values of the torsional springs). To the authors' knowledge, this aspect of the proposed model has not been

employed in the literature. It is also noted that all parameters can be calculated for specific experimental data using the method detailed in this study. When using this method, care must be taken in terms of the placement of the spherical joints since that location must match the origin of the coordinate system with respect to which the experimental data were measured. The predicted response is sensitive to this location and may require additional effort to locate accurately [10].

Though this model was derived to acquire anatomically-correct motion patterns for a robotic spine, it is general for other pseudo-static lumbar spine biomechanical applications. For example, the model predicts the displacement of any point on any lumbar vertebra, useful in studies of lumbar spine muscles length changes.

There are limitations to the model. First, this model would not be reliable for motions with high accelerations, which require inertial forces, ignored in the proposed model and the referenced experimental data. Second, combined motion of the lumbar spine is not addressed in this model, requiring application of external moments about more than one axis. Accelerated and/or combined motions are seldom utilized during clinical diagnoses. The results are satisfactory for programming the RLS since it targets training medical students.

The palpation of muscles and soft tissue is significant for palpatory diagnosis. The forces of the spinal muscles can be incorporated into the model applying a force generation model and considering the attachment points on the bones and tendons. However, deciding how the muscles would "feel" like (when touched by a physician) between those attachment points would be a quite involved task. The ultimate goal of this model was to produce the angles of rotations to be commanded to the robotic lumbar spine as realistically as possible. Upon building the robotic lumbar spine, the addition of the muscles and soft tissue will be performed with strong collaboration of the faculty from the College of Osteopathic Medicine at Ohio University. We have been working with DOs for a long time in matters that require their feedback in terms of how normal or dysfunctional tissue would feel like. In the past, we have had success in developing virtual training simulations using their valuable feedback.

The RLS will be programmed to be controlled by a force-feedback joystick. Via joystick motion, the angles of rotations from this study will be commanded to the RLS, representing normal lumbar spine movement. Abnormalities from known dysfunctional movement patterns will also be enabled.

In conclusion, a three-dimensional mathematical model to estimate the normal movement patterns of the lumbar spine under different loading conditions was proposed. This model will be used in programming of a cable-actuated Robotic Lumbar Spine for training of medical students to identify normal and abnormal movement patterns. Model parameters were obtained by using previously-published experimental data and results validation showed good agreement.

References

[1] Karadogan E., Williams II R.L., 2010, "A Cable-Actuated Robotic Lumbar Spine for Palpatory Training of Medical Students," CD Proceedings of the ASME International Design Technical Conferences, 34th Mechanisms And Robotics Conference, Paper # DETC2010-28863, Montreal, Quebec, Canada, August 15-18.

[2] Panjabi M.M., 1973, "Three -dimensional mathematical model of the human spine structure," Journal of Biomechanics, 6, pp. 671-680.

[3] Soni, A.H., Sullivan J.A. Jr., Patwardhan A.G., Gudavalli M.R., Chitwood J., 1982, "Kinematic analysis and simulation of vertebral motion under static load - Part I: Kinematic Analysis," Journal of Biomechanical Engineering, 104 (2), pp. 105-11.

[4] Lavaste F., Skalli W., Robin S., Roy-Camille R., Mazel C., 1992, "Three-dimensional geometrical and mechanical modeling of the lumbar spine," Journal of Biomechanics, 25, pp. 1153–64.

[5] Cheng, C. and Kumar, S., 1991., "A three-dimensional static torso model for the six human lumbar joints," International Journal of Industrial Ergonomics, 7, pp. 327–339.

[6] Case, K., Xiao, D., Acar, B.S. and Porter, J.M., 1999, "Computer-aided modeling of the Human Spine," Proceedings of the Institution of Mechanical Engineers, Journal of Manufacturing, 213, pp. 83-86.

[7] Cholewicki J., Crisco, J. J., Oxland T. R., Yamamoto I., Panjabi M. M., 1996, "Effects of posture and structure on three-dimensional coupled rotations in the lumbar spine. A biomechanical analysis," Spine, 21(21), pp. 2421-8.

[8] Belytschko T.B., Andriacchi T.P., Schultz A.B., Galante J.O., 1973, "Analog studies of forces in the human spine: computational techniques," Journal of Biomechanics, 6(4), pp. 361-71.

[9] Schultz A.B., Belytschko T.B., Andriacchi T.P., Galante J.O., 1973, "Analog studies of forces in the human spine: mechanical properties and motion segment behavior," Journal of Biomechanics, 6(4), pp. 373-383.

[10] Patwardhan A.G., Soni, A.H., Sullivan J.A. Jr., Gudavalli M.R., Srinivasan V., 1982, "Kinematic analysis and simulation of vertebral motion under static load - Part II: Simulation Study," Journal of Biomechanical Engineering, 104(2), pp. 105-11.

[11] Sullivan, J.A., Soni, A.H., Patwardhan, A.G., Oct. 1979, "Kinematic analysis of intervertebral motion of the human lumbar spine," Final report submitted to OREF.

[12] Sharma M., Langrana N.A., Rodriguez J., 1998, "Modeling of facet articulation as a nonlinear moving contact problem: Sensitivity study on lumbar facet response," Journal of Biomechanical Engineering, 120(1), pp. 118-25.

[13] Panjabi M.M., Oxland T.R., Yamamoto I., Crisco J.J., 1994, "Mechanical behavior of the human lumbar and lumbosacral spine as shown by three-dimensional load-displacement curves," J Bone Joint Surg Am., 76, pp. 413-424.

[14] Karadogan E., 2011, "A Cable-Actuated Robotic Lumbar Spine as the Haptic Interface for Palpatory Training of Medical Students," Ph.D. thesis, Ohio University, Athens, OH.

[15] Adams M.A., Hutton W.C., Stott JR.R., 1980, "The resistance to flexion of the lumbar intervertebral joint," Spine, 5, pp. 245-53.

[16] Zander T., Rohlmann A., Bergmann G., 2004, "Influence of ligament stiffness on the mechanical behaviour of a functional spinal unit," Journal of Biomechanics, 37, pp. 1107-1111.